A Newton-like Finite Element Scheme for Compressible Gas Flows

Marcel Gurris[a], Dmitri Kuzmin[b], Stefan Turek[a]

[a] *Dortmund University of Technology, Institute of Applied Mathematics*
Vogelpothsweg 87, D-44227 Dortmund, Germany
[b] *University of Houston, Department of Mathematics*
651 PGH, Houston, TX 77204-3008, USA

Abstract

Semi-implicit and Newton-like finite element methods are developed for the stationary compressible Euler equations. The Galerkin discretization of the inviscid fluxes is potentially oscillatory and unstable. To suppress numerical oscillations, the spatial discretization is performed by a high-resolution finite element scheme based on algebraic flux correction. A multidimensional limiter of TVD type is employed. An important goal is the efficient computation of stationary solutions in a wide range of Mach numbers, which is a challenging task due to oscillatory correction factors associated with TVD-type flux limiters. A semi-implicit scheme is derived by a time-lagged linearization of the nonlinear residual, and a Newton-like method is obtained in the limit of infinite CFL numbers. Special emphasis is laid on the numerical treatment of weakly imposed characteristic boundary conditions. It is shown that the proposed approach offers unconditional stability as well as higher accuracy and better convergence behavior than in the case of algorithms in which the boundary conditions are implemented in a strong sense.

Keywords: compressible Euler equations, steady-state solutions, finite elements, high-resolution schemes, algebraic flux correction, boundary conditions

1. Introduction

In recent years, significant advances have been made in the development of numerical methods for convection-dominated transport problems. In particular, Kuzmin et al. [7, 8, 9, 6, 11] have developed a new approach to the design of high-resolution finite element schemes. Within the framework of *algebraic flux correction*, the coefficients of a standard Galerkin discretization are constrained using flux limiters based on a generalization of flux-corrected transport (FCT) algorithms and total variation diminishing (TVD) methods. As demonstrated by John and Schmeyer [5], algebraic flux correction is more reliable than mainstream stabilization/shock capturing techniques. The linearized FCT algorithm [6] is to be recommended for transient flows, whereas flux limiters of TVD type are better suited for the computation of steady-state solutions which is of primary interest in the present numerical study. Hence, the latter limiting strategy is adopted.

In contrast to their superior approximation properties, TVD-like flux limiters are known to inhibit steady-state convergence [20]. It is not unusual that the stationary residual decreases by a few orders of magnitude, after which convergence stalls due to the oscillatory correction factors. The lack of convergence compromises the advantages of flux limiting and increases the computational cost. Therefore, it is essential to find the reasons for and remedies to the above convergence problems [13]. In real-life applications, the computational mesh is frequently unstructured, and adaptive mesh refinement [14] is a must. This calls for the use of implicit schemes since the time step size in explicit computations is restricted by stability constraints based on the size of the smallest mesh cells. Implicit solvers are still rarely used for the computation of stationary solutions

to the Euler equations. Their development has been pursued by several groups [1, 2, 15, 19], and various improvements have been proposed to circumvent the stability restrictions of explicit schemes. However, many existing schemes employ linearizable/differentiable limiters, are conditionally stable, and the rate of steady-state convergence deteriorates if the CFL number exceeds a certain upper bound.

Boundary conditions are an important part of the flow solver, and sufficient care must be taken in their numerical implementation. The accuracy, robustness, stability, and convergence of an implicit solver are strongly influenced by the boundary treatment. As shown in [3], strongly imposed boundary conditions may inhibit convergence to a steady state. Thus, it is worthwhile to use flux boundary conditions of Neumann type. To this end, a boundary Riemann solver is incorporated into the weak form of the Galerkin discretization. Similar weak boundary conditions without a boundary Riemann solver were employed in [1, 12].

In the following sections, we address the design of high-resolution finite element schemes for the Euler equations. In particular, the treatment of boundary conditions is described, and the implicit solver is presented. Furthermore, we illustrate the steady-state convergence behavior of the proposed algorithm by numerical results and perform a grid convergence study to examine the spatial accuracy.

2. Finite Element Discretization

The compressible Euler equations represent a system of conservation laws for the mass, momentum, and energy. The divergence form of this system reads

$$\partial_t U + \nabla \cdot \mathbf{F}(U) = 0 \qquad \text{in } \Omega, \tag{1}$$

where U is the vector of conserved quantities and $\mathbf{F}(U)$ is the matrix of fluxes.

In this paper, we discretize (1) in space using continuous finite elements. Let $\{\varphi_i : i = 1, \ldots, NVT\}$ be a set of piecewise linear or bilinear basis functions associated with the vertices of the mesh. The group finite element approximation

$$U_h = \sum_j U_j \varphi_j, \quad \mathbf{F}_h = \sum_j \mathbf{F}_j \varphi_j$$

yields a system of differential-algebraic equations for the nodal values of U_h [10]

$$\sum_j \left[\int_\Omega \varphi_i \varphi_j \, d\mathbf{x} \right] \frac{dU_j}{dt} + \sum_j \left[\int_\Omega \varphi_i \nabla \varphi_j \, d\mathbf{x} \right] \cdot \mathbf{F}_j = 0 \quad \forall i. \tag{2}$$

The above Galerkin discretization is second-order accurate and globally conservative. It can be written in the compact matrix form

$$\sum_j m_{ij} \frac{dU_j}{dt} = -\sum_j \mathbf{c}_{ij} \cdot \mathbf{F}_j \qquad \text{or} \qquad M_C \frac{dU}{dt} = KU, \tag{3}$$

where M_C denotes the consistent block mass matrix and K is the discrete transport operator. The coefficients of this finite element scheme are given by

$$m_{ij} = \int_\Omega \varphi_i \varphi_j \, d\mathbf{x} \qquad \text{and} \qquad \mathbf{c}_{ij} = \int_\Omega \varphi_i \nabla \varphi_j \, d\mathbf{x}. \tag{4}$$

To impose boundary conditions in a weak sense, we integrate equation (3) by parts, which gives rise to a surface integral in the weak formulation

$$\sum_j m_{ij}\frac{dU_j}{dt} = \sum_j \mathbf{c}_{ji}\cdot\mathbf{F}_j - \int_{\partial\Omega}\varphi_i\mathbf{F}_h\cdot\mathbf{n}\,ds, \tag{5}$$

where $\mathbf{n}$ is the unit outward normal to the boundary $\partial\Omega$ of the computational domain Ω. The matrix form of the semi-discrete problem remains unchanged.

3. Algebraic Flux Correction

The standard Galerkin method is known to violate the discrete maximum principle whenever small scale features cannot be resolved properly on a given mesh. To prevent the formation of spurious oscillations and numerical instabilities, we constrain (3) using algebraic flux correction of TVD type. The result is a nonlinear blend of high- and low-order approximations. The latter is defined by

$$M_L\frac{dU}{dt} = LU, \qquad L = K + D, \tag{6}$$

where M_L is the lumped mass matrix and D is an artificial viscosity operator designed so as to render all off-diagonal blocks of L positive semi-definite [3, 10, 14].

The above low-order scheme does not incorporate information about the local smoothness of the solution. Since there is no need for adding artificial viscosity in smooth flow regions, a limited antidiffusive correction F^* is applied to the modified Galerkin operator. The definition of F^* and its practical computation are explained in [3, 8, 14]. The matrix form of the semi-discrete problem becomes

$$M_L\frac{dU}{dt} = K^*U, \qquad K^* = L + F^* = K + D + F^*. \tag{7}$$

By construction, this scheme is nonoscillatory and more accurate than (6) but the antidiffusive part F^* is highly nonlinear, and the local order of approximation depends on the properties of the unknown solution. Hence, an iterative solution strategy is required, and severe convergence problems may occur [13]. A proper interplay of the constrained finite element approximation and iterative solvers is a prerequisite for the use of such approximations in general-purpose CFD codes.

4. Boundary Conditions

A suitable implementation of boundary conditions is also an issue of utmost importance. Numerical errors generated at the boundary are transported into the interior of the domain by the incoming waves, which results in a global loss of accuracy. To keep these errors small and achieve unconditional stability, we impose characteristic boundary conditions of Neumann type. Given a Galerkin discretization of the form (5), the solution of a local Riemann problem is used to calculate the normal fluxes $\tilde{\mathbf{F}}_h \cdot \mathbf{n}$ for the evaluation of the boundary integrals

$$\int_{\partial\Omega} \varphi_i \mathbf{F}_h \cdot \mathbf{n}\, ds \qquad \longrightarrow \qquad \int_{\partial\Omega} \varphi_i \tilde{\mathbf{F}}_h \cdot \mathbf{n}\, ds. \tag{8}$$

The weak imposition of boundary conditions is motivated by the success of finite volume and discontinuous Galerkin methods for (systems of) conservation laws. In contrast to strongly imposed boundary conditions, there is no need to modify the set of admissible basis functions, the finite element matrix, and/or the nodal values of the approximate solution. Since the basis function φ_i has a compact support, the above surface integral reduces to that over the union of boundary patches (edges/faces) where $\varphi_i \neq 0$. Therefore, the flux across a given patch can only affect the nodal values at the vertices that belong to this patch.

4.1. Riemann Invariants

In the case of the Euler equations, incoming and outgoing waves may transport information across the boundary in both directions. Hence, the boundary fluxes to be prescribed depend on the interior (calculated) and exterior (prescribed) boundary states. In general, there are four waves associated with the eigenvalues of the diagonalizable Jacobian matrix. The corresponding local characteristic variables

$$W = \{W_1, W_2, W_3, W_4\} \tag{9}$$

are known as the Riemann invariants. If an eigenvalue λ_i is negative, then the i-th wave enters the domain, and a boundary condition for W_i is required. To leave the boundary transparent to outgoing waves, the Riemann invariants associated with $\lambda_i \geq 0$ are calculated using the current values of the numerical solution [1].

4.2. The Boundary Riemann Solver

The simplest way to prescribe weak Neumann-type boundary conditions is to express the boundary fluxes in terms of the Riemann invariants and substitute the characteristic boundary conditions [1, 2, 12]. Sometimes, this straightforward approach gives rise to physical and numerical problems at the boundary. In particular, negative densities and pressures may occur. To prevent the arising of such unphysical states, we define the normal fluxes $\tilde{\mathbf{F}}_h \cdot \mathbf{n}$ for the surface integral (8) using the solution to a boundary Riemann problem, as in finite volume and DG methods.

At each quadrature point $\mathbf{x}_i \in \partial\Omega$, the interior state U_i for the corresponding Riemann problem is given by the current value $U_h(\mathbf{x}_i)$ of the numerical solution.

The characteristic boundary conditions are applied at a fictitious 'ghost' node $\mathbf{x}_\infty$ placed on the outward normal through $\mathbf{x}_i$, see Fig. 1. The resulting exterior state is denoted by U_∞ and calculated using a transformation to the Riemann invariants. The outgoing ones ($\lambda_i \geq 0$) are evaluated using the solution at $\mathbf{x}_i$. The incoming Riemann invariants ($\lambda_i < 0$) are overwritten by the prescribed boundary conditions. Finally, the result is transformed back to the conservative variables.

In this paper, we calculate $\tilde{\mathbf{F}}_h \cdot \mathbf{n}$ using Roe's approximate Riemann solver

$$\tilde{\mathbf{F}}_h \cdot \mathbf{n} = \frac{1}{2}(\mathbf{F}(U_i) + \mathbf{F}(U_\infty)) \cdot \mathbf{n} - \frac{1}{2}|A^n_{i\infty}|(U_\infty - U_i), \tag{10}$$

where

$$|A^n_{i\infty}| = R^n_{i\infty}|\Lambda^n_{i\infty}|\left[R^n_{i\infty}\right]^{-1}. \tag{11}$$

The eigenvalues $\Lambda^n_{i\infty}$ and eigenvectors $R^n_{i\infty}$ of the 1D Roe matrix $A^n_{i\infty}$ are evaluated using the normal component of the velocity $\mathbf{v}$. In the remainder of this section, we discuss the definition of the ghost state U_∞ for different types of boundaries.

4.3. Inflow and Outflow Boundary Conditions

At the inlet ($\mathbf{v} \cdot \mathbf{n} < 0$) and outlet ($\mathbf{v} \cdot \mathbf{n} > 0$), the characteristic boundary conditions are incorporated into the vector of free stream Riemann invariants

$$W_\infty = \{W_{\infty,1}, W_{\infty,2}, W_{\infty,3}, W_{\infty,4}\}. \tag{12}$$

Depending on the sign of the characteristic wave speed λ_i, the ghost state U_∞ is defined using the prescribed free stream Riemann invariant (if $\lambda_i < 0$) or the value of W_i at the quadrature point (if $\lambda_i \geq 0$). An algorithm that determines the right value of the boundary state automatically can be found in [3]. Sometimes,

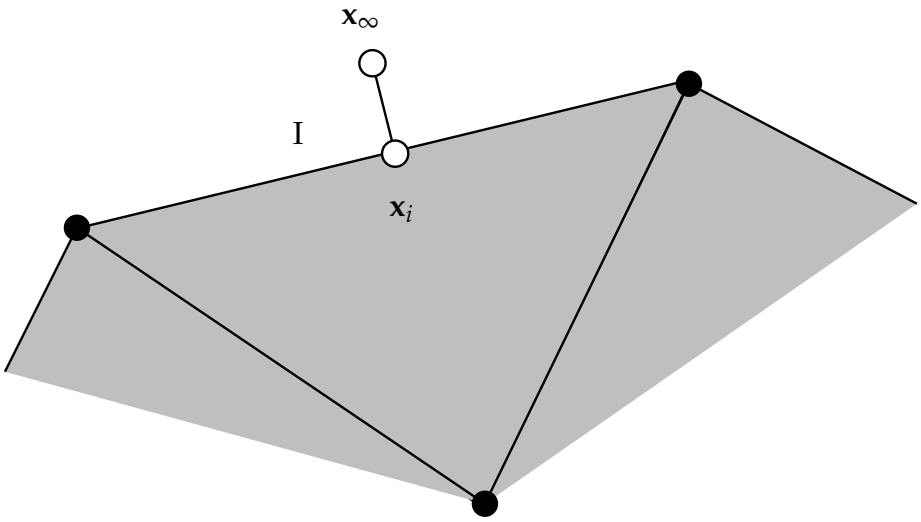

Figure 1: Ghost node and quadrature point

inflow and/or outflow boundary conditions are given in terms of the primitive variables. For example, the pressure is frequently prescribed at a subsonic outlet. The practical implementation of such boundary conditions is discussed in [4, 17].

4.4. Wall Boundary Conditions

At a solid wall, the normal velocity component is zero but the tangential velocity may be non-vanishing. The no-penetration / free-slip boundary condition

$$\mathbf{v} \cdot \mathbf{n} = 0 \tag{13}$$

implies that there is no convective flux of mass, momentum, or energy across the wall. Hence, the weak form of this wall boundary condition is given by

$$\tilde{\mathbf{F}}_h \cdot \mathbf{n} = \begin{bmatrix} 0 \\ \mathbf{n}P \\ 0 \end{bmatrix}, \tag{14}$$

where P is the pressure. Alternatively, the reflecting wall boundary condition

$$\rho_\infty = \rho_i, \qquad v_{n\infty} = -v_{ni}, \qquad v_{\tau\infty} = v_{\tau i}, \qquad E_\infty = E_i \tag{15}$$

can be employed to define the ghost state U_∞ for Roe's approximate Riemann solver (10). The transformation to the conservative variables yields

$$\begin{aligned} \rho_\infty &= \rho_i \\ (\rho\mathbf{v})_\infty &= \rho_\infty(-v_{ni}\mathbf{n} + v_{\tau i}\boldsymbol{\tau}) \\ (\rho E)_\infty &= (\rho E)_i. \end{aligned} \tag{16}$$

In most cases, the two forms of the weakly imposed free-slip condition yield comparable results. The zero-flux condition (14) does not involve a boundary Riemann solver and is sometimes more stable. On the other hand, the mirror condition (16) is slightly more accurate [3]. In this paper, we favor the latter approach.

5. The Semi-Implicit Solver

In steady-state computations, unconditionally stable implicit methods are typically more robust and efficient than explicit algorithms. In particular, the backward Euler scheme is frequently used as an iterative solver for stationary flow

problems. At each pseudo-time step, the numerical solution to the Euler equations is updated by solving a nonlinear algebraic system of the form

$$M_L \frac{U^{n+1} - U^n}{\Delta t} = R^{n+1}, \tag{17}$$

where Δt is a constant time step size. Since accuracy of the converged solution U does not depend on the history of pseudo-time integration, it is worthwhile to choose Δt as large as possible for efficiency reasons. However, this might increase the number of outer iterations for solving (17), or even inhibit convergence.

To avoid the need for solving multiple linear systems per time step, we linearize (17) using a first-order Taylor series expansion of R^{n+1} about U^n, as proposed by Feistauer et al. [1, 2] in the context of discontinuous Galerkin methods

$$\left[\frac{M_L}{\Delta t} - \left(\frac{\partial R}{\partial U} \right)^n \right] (U^{n+1} - U^n) = R^n. \tag{18}$$

This semi-implicit scheme can be interpreted as an implicit underrelaxation of Newton's method [3] which is recovered for a time step of infinite length

$$- \left(\frac{\partial R}{\partial U} \right)^n (U^{n+1} - U^n) = R^n. \tag{19}$$

There is strong numerical evidence that the semi-implicit scheme (18) is unconditionally stable, even for the strongly nonlinear FEM-TVD discretization of the Euler equations. However, a sufficiently accurate initial guess is required to get started. A usable approximation can be computed with the low-order scheme (6).

At the first pseudo-time step, the solution is initialized by extending the inflow boundary condition into the interior of the domain. After a few iterations at moderate CFL numbers, the pseudo-time step can be increased to an arbitrarily large value. The computation of the low-order solution is very cheap compared to the total cost of a steady-state simulation (see Fig. 3). Therefore, the low-order scheme is employed to obtain the initial guess in the numerical study reported below.

5.1. Approximation of the Jacobian

A considerable practical difficulty is the determination of the flux Jacobian for the semi-implicit FEM-TVD solver. Since the limiter function and the correction factors are non-differentiable, no analytical formula for the Jacobian is available. There are several approaches to computing an approximation to be used as a preconditioner in stationary applications. In some publications, the involved derivatives are approximated by finite differences [14, 15] . A major drawback of this methodology is the presence of a free parameter that requires careful fine-tuning.

Another popular approach to Jacobian assembly is automatic differentiation (AD) in the process of residual assembly. When flux or slope limiters are employed, the use of AD tools or (semi-)analytical differentiation is only possible if non-differentiable functions (maxima and minima) are replaced by smooth approximations [13], at least for the purpose of preconditioning. Moreover, the approximate Jacobian matrix may possess unfavorable properties, and its stencil is wider than that of the original Galerkin scheme and of its low-order counterpart.

In light of the above, it is worthwhile to use the Jacobian of the low-order scheme as a preconditioner for the non-differentiable FEM-TVD discretization. If the con-

tribution of the flux limiter is neglected, then the favorable matrix properties are preserved, and each linear system can be solved in an efficient manner. By construction, the residual of the low-order approximation at node i is given by

$$R_i^{low} = \sum_j \mathbf{c}_{ji} \cdot \mathbf{F}_j - \underbrace{\int_{\partial\Omega} \varphi_i \tilde{\mathbf{F}}_h \cdot \mathbf{n}\, ds}_{B_i} + \sum_{j \neq i} D_{ij}(U_j - U_i). \tag{20}$$

The first two terms in the right-hand side of this equation represent the Galerkin discretization. Treating D_{ij} as constant, one obtains the approximate Jacobian

$$\frac{\partial R_i^{low}}{\partial U_j} = \mathbf{c}_{ji} \cdot \frac{\partial \mathbf{F}_j}{\partial U_j} - \frac{\partial B_i}{\partial U_j} + D_{ij}, \qquad \frac{\partial R_i^{low}}{\partial U_i} = \mathbf{c}_{ii} \cdot \frac{\partial \mathbf{F}_i}{\partial U_i} - \frac{\partial B_i}{\partial U_i} - D_{ij}. \tag{21}$$

Since the coefficients $\mathbf{c}_{ji}$ are independent of the solution, the contribution of the Galerkin discretization is exact if the derivatives of the boundary integral B_i are known. A formula for approximation of these derivatives is derived in [3]. It is important to build them into the preconditioner. Otherwise, the large discrepancy between the approximate and exact Jacobians may result in slow convergence.

6. Numerical Results

In this section, we investigate the steady-state convergence behavior of the proposed schemes and perform grid convergence studies. Additional validation can be found in [3]. To apply local time-stepping, we define the time step Δt by

$$\Delta t = \frac{CFL}{\lambda_{max}} h, \tag{22}$$

where h denotes the (local) mesh size, λ_{max} is the largest characteristic speed, and CFL is the prescribed Courant number which has the same value for all nodes.

A well-documented test problem for the Euler equations is the flow past a NACA 0012 airfoil at free stream Mach number $M = 0.8$ and inclination angle $\alpha = 1.25°$. A hierarchy of four triangular meshes is employed. The mesh properties are listed in Table 1. The computation of a low-order predictor begins with a few pre-iterations at $CFL = 10$. When the relative residual drops to approximately 10^{-2}, the CFL number is increased. The low-order solution serves as initial guess for the computation of the flux-limited Galerkin approximation.

Figure 2 displays the numerical solution computed by the high-resolution scheme on the finest mesh (level four). The empirical order of grid convergence

$$p \approx \frac{\frac{\|U_h - U_{ref}\|_2}{\|U_{h/2} - U_{ref}\|_2}}{\log(2)} \tag{23}$$

was determined both for the low-order scheme and for its flux-corrected counterpart. The reference solution U_{ref} was calculated using the latter method on mesh level four. The numerical errors were measured in the relative L_2-norm

$$E_2 = \frac{\|U_h - U_{ref}\|_2}{\|U_{ref}\|_2}. \tag{24}$$

The results in Table 1 indicate that the order of accuracy of the FEM-TVD scheme is about $p^{Lim} \approx 1$. The rate of grid convergence of the low-order scheme is $p^{Low} \approx 0.5$. Similar estimates were obtained by Sokolichin [18] for 1D convection. Note that second-order accuracy cannot be expected due to the presence of shocks. The transonic flow pattern is illustrated by the Mach number isolines in Fig. 2.

Level	Vertices	Elements	E_2^{Low}	p^{Low}	E_2^{Lim}	p^{Lim}
1	2577	4963	$4.08 \cdot 10^{-2}$	0.51	$1.68 \cdot 10^{-3}$	1.02
2	10117	19852	$2.86 \cdot 10^{-2}$	0.46	$8.27 \cdot 10^{-4}$	1.02
3	40086	79408	$2.08 \cdot 10^{-2}$		$2.68 \cdot 10^{-4}$	
4	159580	317632				

Table 1: NACA airfoil: Mesh properties and error analysis

The steady-state convergence history of the two schemes is reported in Fig. 3. The convergence rates of the low-order scheme improve with increasing CFL numbers, and the relative error falls below 10^{-14} in about 20 iterations. This illustrates the benefits of implementing boundary conditions in a weak sense. The FEM-TVD scheme exhibits similar convergence behavior, although much more iterations are required to approach the steady state. Despite oscillatory correction factors, which are usually blamed for the lack of convergence [13], the relative error falls below 10^{-8} after about 200 iterations. The scheme appears to be unconditionally stable, so that there is no need to determine the largest admissible time step by trial and error. In contrast to the findings reported in [19], no deterioration of convergence rates is observed at large CFL numbers. In fact, the use of larger time steps results in faster convergence, although the improvement is marginal for $CFL \geq 100$.

7. Conclusions and Outlook

A high-resolution finite element scheme was proposed for the compressible Euler equations. The main highlight is a robust iterative solver that delivers converged steady-state solutions despite oscillatory correction factors. The semi-implicit pseudo-time-stepping appears to be unconditionally stable and reduces to a Newton-like method in the limit of infinite CFL numbers. The convergence

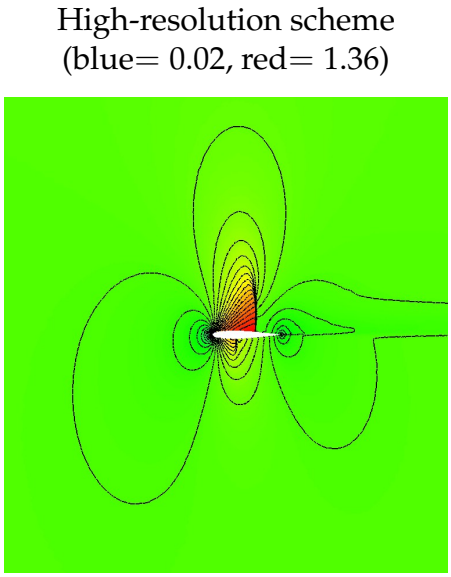

Figure 2: NACA airfoil: Mach number zoom (40 contours)

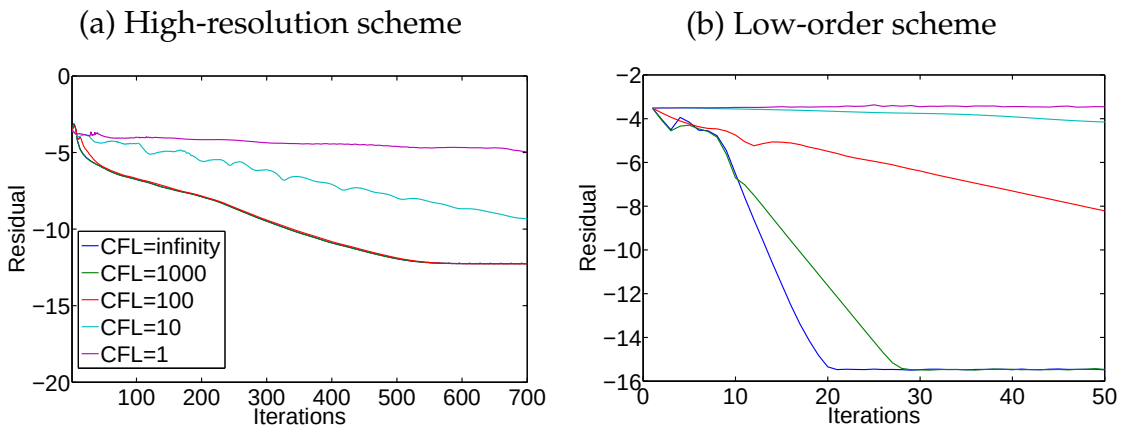

Figure 3: NACA airfoil: Nonlinear convergence history in logarithmic scale for different CFL numbers on mesh level two

rates improve with increasing time steps and do not deteriorate if the CFL number exceeds some upper bound. The Galerkin finite element discretization was equipped with weak boundary conditions of Neumann type. Their accuracy was demonstrated by a grid convergence study. The high-resolution scheme based on a multidimensional flux limiter of TVD type was shown to converge twice as fast as its low-order counterpart, even in the case of discontinuous weak solutions.

The convergence to steady state can be further accelerated within the framework of a nonlinear (FAS-FMG) multigrid method. Further tasks to be accomplished include the implementation of the new algorithm in 3D, its combination with adaptive mesh refinement techniques, and application to real-life problems.

Acknowledgement

The authors gratefully acknowledge the financial support by the DFG (German Research Foundation, SFB 708).

References

[1] V. Dolejší, M. Feistauer: *A semi-implicit discontinuous Galerkin finite element method for the numerical solution of inviscid compressible flow*, J. Comp. Phys., Vol. 198, 2004, pp. 727-746.

[2] M. Feistauer, V. Kučera: *On a robust discontinuous Galerkin technique for the solution of compressible flow*, J. Comput. Phys., Vol. 224, 2007, pp. 208–221.

[3] M. Gurris: *Implicit Finite Element Schemes for Compressible Gas and Particle-Laden Gas Flows*, PhD Thesis, Dortmund, 2009.

[4] C. Hirsch: *Numerical Computation of Internal and External Flows: Computational Methods for Inviscid and Viscous Flows*, Vol. II, John Wiley and Sons, New York, 1990.

[5] V. John, E. Schmeyer: *Finite element methods for time-dependent convection-diffusion-reaction equations with small diffusion*, Comput. Meth. Appl. Mech. Eng., Vol 198, 2008, pp. 475-494.

[6] D. Kuzmin: *Explicit and implicit FEM-FCT algorithms with flux linearization*, J. Comput. Phys., Vol. 228, 2009, pp. 2517–2534.

[7] D. Kuzmin: *On the design of general purpose flux limiters for finite element schemes. I. Scalar convection*, J. Comp. Phys., Vol. 219, 2006, pp. 513-531.

[8] D. Kuzmin: *Algebraic flux correction for finite element discretizations of coupled systems*, In E. Onate, M. Papadrakakis, B. Schrefler, editors, Comp. Meth. for Coupled Prob. in Sc. and. Eng. II, CIMNE, 2007, pp. 653-656.

[9] D. Kuzmin, M. Möller: *Algebraic flux correction I. Scalar conservation laws*, In D. Kuzmin, R. Löhner, S. Turek, editors, Flux-Corrected Transport, Principles, Algorithms, and Applications, pp. 155-206, Springer, 2005.

[10] D. Kuzmin, M. Möller: *Algebraic flux correction II. Compressible Euler equations*, In D. Kuzmin, R. Löhner, S. Turek, editors, Flux-Corrected Transport, Principles, Algorithms, and Applications, pp. 207-250, Springer, 2005.

[11] D. Kuzmin, S. Turek: *High-resolution FEM-TVD schemes based on a fully multidimensional flux limiter*, J. Comp. Phys., Vol. 198 (1), 2004, pp. 131-158.

[12] V. Selmin, L. Formaggia: *Unified construction of finite element and finite volume discretizations for compressible flows*, Int. J. Num. Meth. Eng., Vol. 39, 1996, pp. 1-32.

[13] K. Michalak, C. Ollivier Gooch: *Differentiability of Slope Limiters on Unstructured Grids*, In: Proceedings of Fourteenth Annual Conference of the Computational Fluid Dynamics Society of Canada, 2006.

[14] M. Möller: *Adaptive High-Resolution Finite Element Schemes*, PhD Thesis, TU Dortmund, 2008.

[15] A. Nejat: *A Higher-Order Accurate Unstructured Finite Volume Newton-Krylov Algorithm for Inviscid Compressible Flows*, PhD Thesis, Vancouver, 2007.

[16] P. L. Roe: *Approximate Riemann solvers, parameter vectors and difference schemes*, J. Comp. Phys., Vol. 43, 1981, pp. 357-372.

[17] R. A. Shapiro: *An Adaptive Finite Element Solution Algorithm for the Compressible Euler Equations*, PhD Thesis, Massachusetts, 1988.

[18] A. Sokolichin: *Mathematische Modellbildung und Numerische Simulation von Gas-Flüssigkeits-Blasenströmungen*, (German), Habilitation Thesis, Stuttgart, 2002.

[19] J.-Y. Trépanier, M. Reggio, D. Ait-Ali-Yahia: *An implicit flux-difference splitting method for solving the Euler equations on adaptive triangular grids*, Int. J. Num. Meth. Heat Fluid Flow, Vol. 3, 1993, pp. 63-77.

[20] D. L. Whitaker, D. C. Slack, R. W. Walters: *Solution algorithms for the two-dimensional Euler equations on unstructured meshes*, AIAA Paper, 1990, Article No. 90-0697.